Cellular/Molecular

Rescue of Normal Excitability in LGI1-Deficient Epileptic Neurons

Johanna Extrémet,[1] Jorge Ramirez-Franco,[1] Laure Fronzaroli-Molinieres,[1] Norah Boumedine-Guignon,[1] Norbert Ankri,[1] Oussama El Far,[1] Juan José Garrido,[2] Dominique Debanne,[1] and Michaël Russier[1]

[1]Unité de Neurobiologie des canaux Ioniques et de la Synapse, Unité Mixte de Recherche 1072, Institut National de la Santé et de la Recherche Médicale, Aix-Marseille Université, Marseille, 13015, France and [2]Cajal Institute, Consejo Superior de Investigaciones Cientificas, Madrid, 28002, Spain

Leucine-rich glioma inactivated 1 (LGI1) is a glycoprotein secreted by neurons, the deletion of which leads to autosomal dominant lateral temporal lobe epilepsy. We previously showed that LGI1 deficiency in a mouse model (i.e., knock-out for LGI1 or KO-Lgi1) decreased Kv1.1 channel density at the axon initial segment (AIS) and at presynaptic terminals, thus enhancing both intrinsic excitability and glutamate release. However, it is not known whether normal excitability can be restored in epileptic neurons. Here, we show that the selective expression of LGI1 in KO-Lgi1 neurons from mice of both sexes, using single-cell electroporation, reduces intrinsic excitability and restores both the Kv1.1-mediated D-type current and Kv1.1 channels at the AIS. In addition, we show that the homeostatic-like shortening of the AIS length observed in KO-Lgi1 neurons is prevented in neurons electroporated with the Lgi1 gene. Furthermore, we reveal a spatial gradient of intrinsic excitability that is centered on the electroporated neuron. We conclude that expression of LGI1 restores normal excitability through functional Kv1 channels at the AIS.

Key words: epilepsy; excitability; hippocampus; Kv1 channel; LGI1

Significance Statement

The lack of leucine-rich glioma inactivated 1 (LGI1) protein induces severe epileptic seizures that leads to death. Enhanced intrinsic and synaptic excitation in KO-Lgi1 mice is because of the decrease in Kv1.1 channels in CA3 neurons. However, the conditions to restore normal excitability profile in epileptic neurons remain to be defined. We show here that the expression of LGI1 in KO-Lgi1 neurons in single neurons reduces intrinsic excitability, and restores both the Kv1.1-mediated D-type current and Kv1.1 channels at the axon initial segment (AIS). Furthermore, the homeostatic shortening of the AIS length observed in KO-Lgi1 neurons is prevented in neurons in which the Lgi1 gene has been rescued. We conclude that LGI1 constitutes a critical factor to restore normal excitability in epileptic neurons.

Introduction

Leucine-rich glioma inactivated (LGI1) composed of a leucine-rich repeat (LRR) domain and an epitempin (EPTP) domain is a secreted protein expressed primarily in the CNS. Several genes coding for proteins with EPTP domain are found in genomic

region associated with epilepsy (Staub et al., 2002). The deletion of LGI1 protein induces autosomal dominant lateral and temporal lobe epilepsy (ADLTE), a pathology characterized by epileptic seizures with auditory disorders (Kalachikov et al., 2002). ADLTE can be induced by homozygous deletion of LGI1 in mice (Lgi1 knock-out mice or KO-Lgi1 mice). LGI1 functionality requires the binding to the disintegrin and metalloproteinase domain-containing protein 22 (ADAM22), a noncatalytic metalloprotease-like protein which act as a receptor for LGI1. Most of Lgi1 mutations prevent LGI1 secretion while secretion permissive mutations have been shown to disrupt its interaction with ADAM22 (Yokoi et al., 2015; Yamagata et al., 2018). Subsequent loss of LGI1 function in these mice induces epileptiform activities, seizures and premature death (Chabrol et al., 2010).

The mechanisms by which the epileptic phenotype occurs in KO-Lgi1 mice involve changes in excitatory synaptic transmission (Fukata et al., 2006, 2010; Lovero et al., 2015; Boillot et al., 2016), synapse maturation (Y.D. Zhou et al., 2009; Lovero et al., 2015; Thomas et al., 2018), and also changes in intrinsic

excitability (Schulte et al., 2006; Seagar et al., 2017; Lugarà et al., 2020). In Kv1.4/Kv1.1 channels, LGI1 prevents N-type inactivation by the Kvβ1 subunit (Schulte et al., 2006). Addition of recombinant LGI1 decreases intrinsic excitability in rat CA3 neurons whereas CA3 neurons of KO-Lgi1 mice are more excitable (Seagar et al., 2017). In fact, LGI1 tunes neuronal excitability by controlling the expression of voltage-gated Kv1.1-containing potassium channels density at the axon initial segment (AIS) of CA3 pyramidal neurons (Seagar et al., 2017). Accordingly, LGI1 and its receptor ADAM22 are colocalized at the AIS of dissociated hippocampal neurons, thus affecting the Kv1 potassium channel localization in this compartment (Hivert et al., 2019). The slowly inactivating D-type current (I_D) mediated by Kv1 channels dampens action potential firing, and subsequently reduces synchronization of CA3 pyramidal neurons (Cudmore et al., 2010). Moreover, Kv1.1-containing channels present in the AIS have been shown to regulate intrinsic excitability of CA3 neurons (Rama et al., 2017). Consistent with a decrease in Kv1.1 density in CA3 neuron of KO-Lgi1 mice, the conductance of the voltage-gated D-type potassium current carried by the Kv1 channels family was found to be reduced (Seagar et al., 2017).

While rescue experiments have been often conducted to study synaptic mechanisms (Fukata et al., 2010; Lovero et al., 2015), the rescue strategy has not been used to confirm the role of LGI1 in the control of intrinsic excitability. In particular, it is unclear whether the rescue of Lgi1 gene in a single neuron is able to restore D-type potassium conductance and thus normal intrinsic excitability. We show here that selective expression of LGI1 in neurons from KO-Lgi1 mice using single-cell electroporation (SCE) reduces intrinsic excitability and increases both the Kv1.1-mediated D-type current and Kv1.1 immunostaining at the AIS. In addition, we reveal a spatial gradient of intrinsic excitability centered on the electroporated neuron. Thus, the expression of LGI1 restores normal excitability through the expression of functional Kv1 channels at the AIS.

Materials and Methods

Production of KO-Lgi1 mice

All experiments were conducted according to the European and Institutional guidelines for the care and use of laboratory animals (Council Directive 86/609/EEC and French National Research Council) and approved by the local health authority (D13055-08, Préfecture des Bouches du Rhône). Heterozygous Lgi1$^{+/-}$ mice were crossed to generate Lgi1$^{-/-}$ [i.e., knock-out (KO)], Lgi1$^{+/-}$, and Lgi1$^{+/+}$ [wild-type (WT)] littermates. WT and KO mice were selected by analyzing the amplification profile from PCR. After sampling from 7-d-old mice, DNA were denatured by temperature variations with a mix of 0.5 µl of DNA release diluted in 20 µl of dilution buffer (Master mix, ThermoFisher). A total of 1 µl of DNA extraction from each sample was amplified with 0.25 µl of primer (final concentration of 0.3 µM for each primer: WT F, WT R, KO F, KO R; Table 1), 10 µl of Phire containing DNA polymerase (Master mix, ThermoFisher) and 8.75 of water in the Thermal Cycler (ProFlex PCR system, Life Technologies). PCR products were migrating in agarose gel (2%) and the resulting migration bands were visualised at 120 pb (WT band) and 200 pb (KO band) with a biomarker band as a reference.

Hippocampal slice cultures

Slices cultures were prepared as described previously (Debanne et al., 2008; Extrémet et al., 2022). Young Lgi1 KO mice (Postnatal day 7 to 10) were killed by decapitation, the brain was removed, and each hippocampus dissected. Hippocampal slices (350 µm) were obtained using a Vibratome (Leica, VT1200S). They were placed on 20-mm latex membranes (Millicell) inserted into 35 mm Petri dishes containing 1 ml of culture medium and maintained for up to 21 d in an incubator at 34°C,

Table 1. List of primers

LGI1 LOX WT F	5′-ATT TCC TTA GTG CCC CTG TTT TTA-3′
LGI1 LOX WT R	5′-TGT CTG GAT TCA ATG CTG TCT TAG A-3′
LGI1 KO 2 F	5′-ACA TTT CCT TAG TGC CCC TGT TT-3′
LGI1 KO 2 R	5′-CCT CTT AGC CAC TGA GGC ATC T-3′

95% O$_2$–5% CO$_2$. The culture medium contained (in ml) 25 MEM, 12.5 HBSS, 12.5 horse serum, 0.5 penicillin/streptomycin, 0.8 glucose (1 M), 0.1 ascorbic acid (1 mg/ml), 0.4 HEPES (1 M), 0.5 B27, and 8.95 sterile H$_2$O.

Single-cell electroporation

Electroporation-mediated transfection (Rathenberg et al., 2003) was conducted in organotypic slice cultures of mouse hippocampus at 4 d in vitro (DIV). The plasmid pIND-LGI1-IRES-EGFP (Ramirez-Franco et al., 2022) was used to concomitantly express Lgi1 and enhanced green-fluorescence protein (EGFP). In control conditions, we used pIND-IRES-EGFP (Ramirez-Franco et al., 2022) devoid of any Lgi1 expressing sequence. In order to follow extracellular LGI1 secretion, we used a pIND-Δ-IRES-Dendra2-LGI1 that expresses Dendra2-tagged Lgi1 (D2-Lgi1-encoding gene; Ramirez-Franco et al., 2022). In order to identify the morphology of electroporated neurons, we used a tdTomato expressing plasmid (tdTomato-N1; gift from Michael Davidson, Nathan Shaner, and Roger Tsien; Addgene plasmid #54642; http://n2t.net/addgene:54642; RRID: Addgene_54642; Shaner et al., 2004). Before electroporation, plasmid solutions were centrifuged at 10,000 × g for 5 min to avoid obstruction of the micropipette. Immediately after single-cell electroporation, protein expression was induced by adding doxycycline (0.3 µg/ml) to the cell culture (Fig. 1A). Lgi1 and EGFP were expressed for 3 d, and D2-Lgi1 and tdTomato were expressed for 6 d before further processing.

For single-cell electroporation (SCE), the microscope chamber was consisting of a sterile 60-mm Petri dish. The plasmid DNA constructs were diluted to a final concentration of 33 ng/µl in the internal solution containing (in mM): 120 K-gluconate, 20 KCl, 10 HEPES, 0.5 EGTA, 2 MgCl$_2$, 2 Na$_2$ATP, and 0.3 NaGTP (pH 7.4). Micropipettes (7–10 MΩ) were filled with this DNA preparation after filtration with a sterile Acrodisc Syringe Filter (0.2 µm in pore diameter).

During the SCE procedure, slice culture (DIV4–DIV5) was positioned in the 60-mm Petri dish and covered with prewarmed and filtered external solution containing (in mM): 125 NaCl, 26 NaHCO$_3$, 3 CaCl$_2$, 2.5 KCl, 2 MgCl$_2$, 0.8 NaH$_2$PO$_4$, and 10 D-glucose, equilibrated with 95% O$_2$–5% CO$_2$. The ground electrode and the microelectrode were connected to an isolated voltage stimulator (Axoporator 800A, Molecular Devices). Under visual guidance, the micropipette was positioned by a three-axis micromanipulator near the cell body of selected CA3 neurons. Pressure was controlled to have a loose-seal between the micropipette and the plasma membrane. When the resistance monitored reached 25–40 MΩ, we induced a train of −12-V pulses during 500 ms (pulse width: 0.5 ms, frequency: 50 Hz). Each organotypic slice culture underwent SCE procedure for 8–10 selected neurons during a limited time of 30 min and was then back transferred to the incubator.

Electrophysiology

After 3 d in the presence of doxycycline, whole-cell recordings were obtained from electroporated CA3 neurons, which were identified by EGFP expression. Patch pipettes (7–10 MΩ) were filled with the internal solution containing (in mM): 120 K-gluconate, 20 KCl, 10 HEPES, 0.5 EGTA, 2 MgCl$_2$, 2 Na$_2$ATP, and 0.3 NaGTP (pH 7.4). All recordings were made at 29°C in a temperature-controlled recording chamber (Luigs & Neumann GmbH) perfused with the same external solution as for SCE. Liquid junction potential (∼−12 mV) was not compensated in the data reported. Neurons were recorded in current clamp or voltage clamp with a Multiclamp 700B Amplifier (Molecular Devices). Excitability was measured by delivering a range of long (1 s) depolarizing current pulses (10–250 pA, by increments of 10 pA) and counting the number of action potentials. Ionotropic glutamate and GABA receptors were blocked with
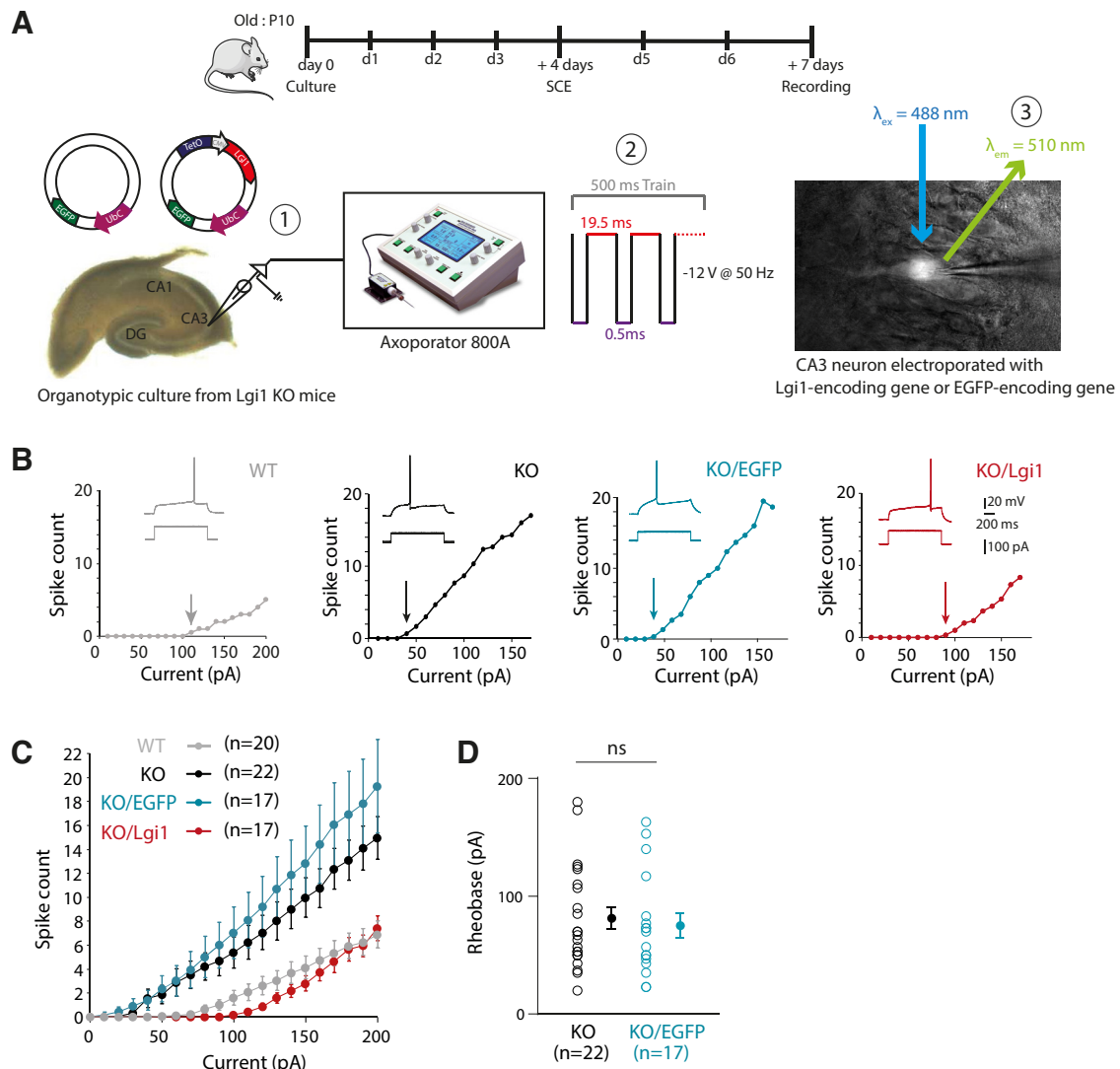
Figure 1. Rescue of intrinsic neuronal excitability in hippocampal CA3 pyramidal neurons from Lgi1 KO mice using SCE of an Lgi1-encoding plasmid. *A*, Scheme of single-cell electroporation procedure. Top, the time course of the experiments (d0...d7 = age of organotypic slices in culture), (1) simplified representation of plasmid DNA constructs (UbC = eGFP constitutive promoter), (2) SCE protocol, and (3) resulting fluorescent electroporated cell. λ_{ex} = excitation wavelength, λ_{em} = emission wavelength. *B*, Input-output curves showing the number of spikes according to depolarizing current increments and corresponding traces of representative neurons from organotypic culture of WT mice (gray), Lgi1 KO mice (black), electroporated with EGFP (blue), or with Lgi1-encoding plasmids (red), respectively. Arrows indicate the rheobase. *C*, Averaged input-output curves in the four cases. *D*, Comparison of the rheobase in KO and KO/EGFP mice. Mann–Whitney test; ns, not significant ($p > 0.05$).

2–4 mm kynurenate and 100 μM picrotoxin, respectively. Input-output curves were determined for each neuron and three parameters were examined: the rheobase (the minimal current eliciting at least one action potential), the gain (measured on each cell as the linear fit of the spike number as a function of current pulse) and the latency of the first spike (depolarizing time before the evoked spike under rheobase current eliciting only 1 spike). Sensitivity to Kv1-channel blocker dendrotoxin K (DTx-K) was determined by current-clamp recording before and after bath application of the DTx-K (100 nM). Voltage-clamp protocols to measure Kv1-channel-mediated currents consisted of a family of voltage-step commands from a holding potential of −90 mV (step from −80 to +10 mV in 10-mV increments). To block voltage dependent Ca^{2+} and Na^{+} currents, 200 μM Ni^{2+}, 50 μM Cd^{2+}, and 0.5 μM TTX were added to the extracellular solution. Algebraic isolation of the D-type potassium current was done by subtracting the currents evoked in the presence of the selective blocker of Kv1.1-containing channel DTx-K, from currents evoked in control solution. The D-type conductance was calculated from the maximal peak of the DTx-k-sensitive current obtained and the driving force of potassium in our recording conditions (electrochemical potential of potassium EK^{+} = −105.09 mV). In all voltage-clamp experiments, leak and

capacitance subtraction was performed using a p/n ($n = 4$) protocol. The voltage and current signals were low-pass filtered (3 and 0.4 kHz, respectively), and acquisition was performed at 10 kHz with pClamp10 (Molecular Devices). Data were analyzed with ClampFit (Molecular Devices) and Igor (Wavemetrics). Spike thresholds were measured using phase plots (Fékété et al., 2021).

Immunohistochemistry
Organotypic cultures from KO-Lgi1 mice were performed as described previously (Ramirez-Franco et al., 2022). Briefly, slices were fixed in a solution containing 4% of paraformaldehyde in PBS for 15 min at 4°C, incubated in 50 mm NH_4Cl in PBS for 15 min at room temperature (RT), and blocked overnight at 4°C in a solution containing 5% normal goat serum (NGS; Vector Laboratories) and 0.5% Triton X-100 in PBS. After blocking, slices were incubated (24 h; 4°C) with primary antibodies in a solution containing 0.5% Triton X-100 and 2% NGS in PBS. The following antibodies were used: guinea pig anti-AnkG (1:400, Synaptic Systems, 386005, RRID: AB_2737033), rabbit anti-EGFP (1:500, Synaptic Systems, 132003, RRID: AB_1834147), mouse anti-Kv1.1 (1:200, Antibodies Incorporated, 75-

105, RRID: AB_10673166) or mouse anti-AnkG (1:400, Antibodies Inc, 75-147, RRID: AB_10675130), rabbit anti-Dendra2 (1:200, Antibodies online, ABIN361314, RRID: AB_10789591), chicken anti-tdTomato (1:500, ThermoFisher, TA150089). The slices were then washed four times for 20 min each time in PBS 0.5% Triton X-100 and then incubated with the appropriate secondary antibodies for 2 h at RT in a solution containing 0.5% Triton X-100 and 2%NGS in PBS. The following antibodies were used: Alexa Fluor 647 goat anti-guinea pig (1:150, Jackson ImmunoResearch), Alexa Fluor 488 goat anti-rabbit (1:200, Jackson ImmunoResearch), Alexa Fluor 594 goat anti-mouse (1:200, Jackson ImmunoResearch), or Alexa Fluor 488 goat anti-rabbit (1:200, Jackson ImmunoResearch), Alexa Fluor 594 donkey anti-chicken (1:400, Jackson ImmunoResearch), Alexa Fluor 647 donkey anti-mouse (1:400, Invitrogen). Subsequently, sections were washed three times for 20 min in PBS 0.5% Triton X-100. Nuclei were stained using DAPI at a final concentration of 1.5 µg/ml in PBS for 10 min and washed in PBS for 15 min. Slices were then mounted in Vectashield mounting medium (Vector Laboratories). Z-stacks of confocal sections were acquired on a LSM780 confocal scanning microscope (Zeiss).

Image processing and quantification
ImageJ (NIH) was used for image analysis and quantification. In order to measure Kv1.1 immunostaining at the AIS, rolling ball background subtraction was performed over the images. Then, object identification was done by using 3D object counter plugin in ImageJ over AnkG signal (Bolte and Cordelières, 2006). After object detection, this 3D mask was applied over Kv1.1 signal or D2-Lgi1 signal, and the 3D ROI manager (Ollion et al., 2013) was used to identify individual AISs within the field of view. Kv1.1 or D2-Lgi1 Immunostaining levels were collected as average gray values. For each condition, Kv1.1 immunostaining at the AIS was normalized to KO neurons away from the neuron electroporated with Lgi1.

In order to overcome differences in EGFP expression between different cells, and since EGFP was only used as a reporter to identify transfected cells, different minimum and maximum display settings were applied for the EGFP channel in some of the images.

AIS length was measured using β4-spectrin staining. Briefly, a line was drawn starting from each soma down to its axon following the β4-spectrin staining. This defines a fluorescence intensity profile along the AIS that increases and then decreases. Starting and end positions of the AIS are defined as the positions where β4-spectrin intensity is detectable.

Statistics
Pooled data are presented as mean $\pm$ SEM and statistical analysis was performed using the Mann–Whitney U test or Wilcoxon rank-signed test. Data were considered statistically significant for $p < 0.05$. For some conditions in electrophysiology and in immunohistochemistry, a resampling was conducted by using the bootstrap method to have comparable samples between distant KO neuron, nearby KO neuron, KO/Lgi1 neurons and KO/EGFP neurons.

Results

Reduced excitability of KO-Lgi1 neurons electroporated with Lgi1-expressing plasmid

To investigate the involvement of LGI1 in shaping neuronal excitability, we rescued its expression in selected CA3 neurons from KO-Lgi1 mice organotypic slice cultures using single cell electroporation of an Lgi1-encoding plasmid (Fig. 1A). A vector allowing expression of the enhanced green-fluorescence protein (EGFP) was used as control to confirm that changes in intrinsic excitability were not because of the single cell electroporation procedure itself (KO/EGFP neurons). CA3 pyramidal neurons were recorded in current-clamp and the number of action potentials for each increment of injected current was counted to establish input-output curves. Excitability parameters (first

spike latency, rheobase, and gain) were measured. No significant difference was observed between KO neurons and KO/EGFP neurons for the first spike latency (671 ± 54 ms, $n = 22$ vs 630 ± 50 ms, $n = 17$, $p = 0.64$), for the rheobase (81 ± 9 pA, $n = 22$ vs 75 ± 11 pA, $n = 17$, $p = 0.65$), nor for the gain (0.11 ± 0.012 spike/pA, $n = 22$ vs 0.12 ± 0.008 spike/pA, $n = 17$, $p = 0.22$).

In contrast to KO/EGFP neurons, KO neurons transfected with Lgi1 encoding plasmid (KO/Lgi1 neurons) expressed a clear ramp-and-delay phenotype that was similar to that of WT neurons (Fig. 1B). According to this characteristic, we measured an increase in the latency of the first spike in CA3 KO/Lgi1 neurons compared with KO/EGFP neurons (630 ± 50 ms, $n = 17$ in control vs 844 ± 27 ms, $n = 17$ in neurons electroporated with Lgi1-encoding plasmid, $p < 0.001$; Fig. 2A). The latency in WT and KO/Lgi1 neurons were similar (Fig. 2A).

Strikingly, the increased first spike latency in CA3 KO/Lgi1 neurons was paralleled with modifications in other excitability parameters. In fact, compared with control KO/EGFP neurons, the input-output curve of CA3 KO/Lgi1 neurons displayed a rightward shift (Fig. 1B,C) with a significant increase in the rheobase (75 ± 11 pA, $n = 17$ vs 136 ± 7 pA, $n = 17$, $p < 0.001$; Fig. 2A), and a significant reduction in the gain (0.12 ± 0.008 spike/pA, $n = 17$ vs 0.08 ± 0.008 spike/pA, $n = 17$, $p < 0.001$; Fig. 2A). Notably the values of rheobase and gain were found to be similar in WT and KO/Lgi1 neurons (Fig. 2A). Furthermore, the voltage threshold of the action potential was found to be significantly depolarized in KO/Lgi1 neurons compared with KO or KO/EGFP neurons (-33 ± 0.5 mV, $n = 17$ in KO/Lgi1 neurons vs -36 ± 0.5 mV, $n = 17$ in KO/EGFP neurons and -35 ± 0.5 mV, $n = 22$ in KO neurons; Fig. 2B). Here again, the spike threshold was found to be comparable in WT and KO/Lgi1 neurons (Fig. 2B). Taken together, these data indicate that intrinsic excitability is reduced in CA3 KO/Lgi1 neurons compared with KO/EGFP, thus showing a rescue of normal intrinsic excitability comparable to the WT control.

Increased sensitivity to DTx-k in KO/Lgi1 neurons

The ramp-and-delay phenotype observed before the evoked spike is a hallmark of slow inactivating D-type current (Cudmore et al., 2010). As this feature was observed in WT and KO/Lgi1 neurons, we examined the contribution of the D-type current to the electrophysiological phenotype after electroporation, by measuring the sensitivity to DTx-k in current-clamp. In WT neurons, application of 100 nM DTx-k induced a clear shift in the input-output curve and a reduction in the first spike latency (Fig. 3A,D). In contrast, only a slight difference was observed in the depolarization preceding the evoked spike (Fig. 3B) with no significant difference in the first spike latency in KO/EGFP neurons after DTx-k application ($n = 6$, $p = 0.52$; Fig. 3D). However, in KO/Lgi1 neurons, bath application of DTx-k induced a loss of the ramp-and-delay phenotype (Fig. 3C) and a significant decrease of the latency to the first spike ($n = 6$, $p = 0.03$; Fig. 3D). According to the input-output curves (Fig. 3B), a slight increase in intrinsic excitability was noticed in KO/EGFP neurons after application of DTx-k. Clearly, the input-output curve of KO/Lgi1 neurons showed a more robust increase of intrinsic excitability after adding DTx-k (Fig. 3C). While DTx-k did not induce changes in the rheobase of KO/EGFP neurons ($n = 6$, $p = 0.44$; Fig. 3D), the rheobase of KO/Lgi1 neurons was significantly decreased after DTx-k application ($n = 6$, $p = 0.03$; Fig. 3D). To quantify this effect, we subtracted
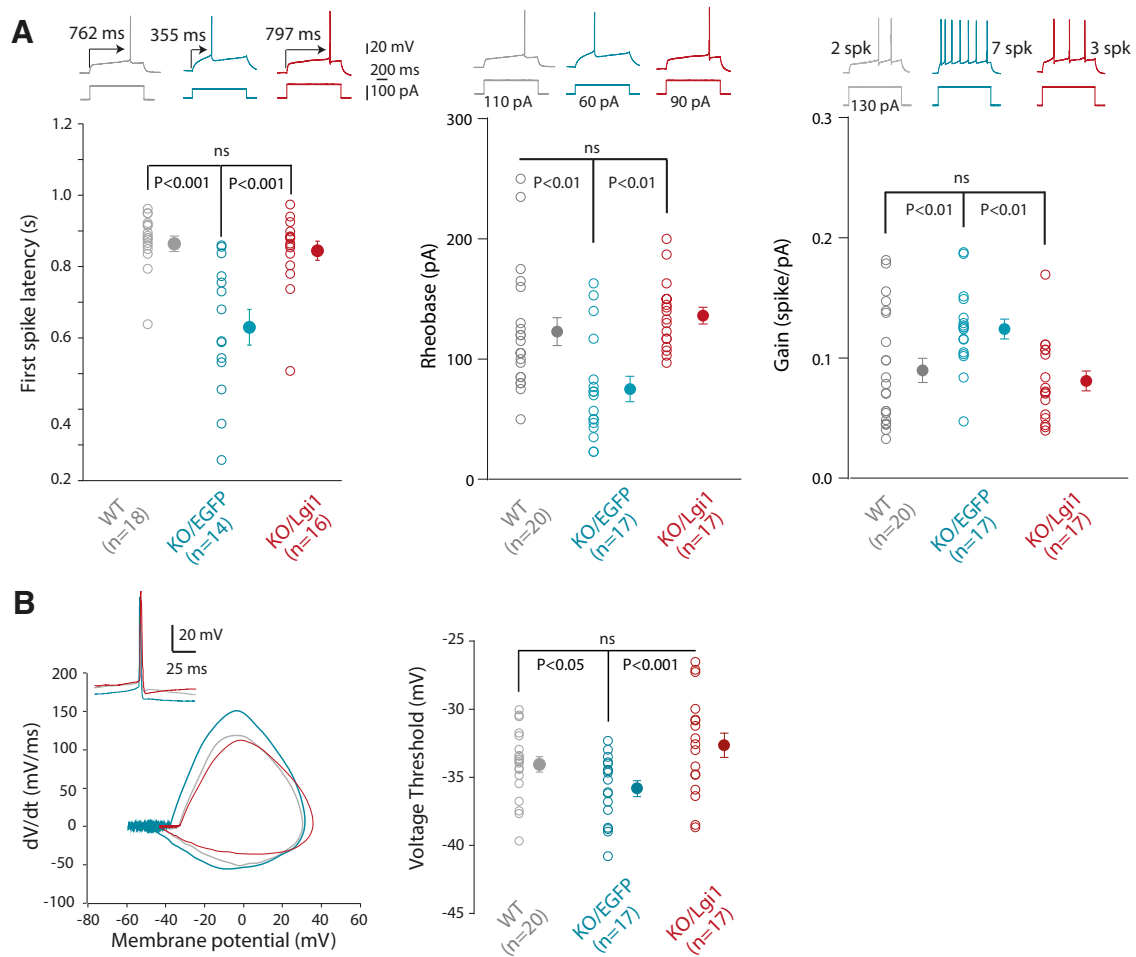
Figure 2. *A*, Left, First spike latency obtained at rheobase current in WT (gray), KO/EGFP (blue), and KO/LGI1 (red) neurons. Middle, Rheobase. Right, Gain. *B*, Changes in spike threshold. Left, Phase plot of action potentials recorded in a WT neuron (gray), electroporated with EGFP (blue), and Lgi1 (red). Right, Pooled data. Error bars represent SEM. Statistical analysis was performed using the Mann–Whitney test and significance was obtained at *p* < 0.05. ns, not significant.

the rheobase measured after application of DTx-k to the rheobase before adding DTx-k. Compared with the KO/EGFP neurons, a 4-fold increase of this rheobase difference was observed in both WT and KO/Lgi1 neurons (17 ± 7 pA, $n = 6$ vs 65 ± 11 pA, $n = 13$, $p = 0.04$ in WT and 67 ± 9 pA, $n = 6$, $p = 0.004$ in KO/LGI1; Fig. 3*D*) confirming a higher sensitivity to DTx-k in neuron rescued with LGI1.

Recovery of the D-type current and Kv1.1 channels at the AIS of KO/Lgi1 neurons

To confirm the recovery of D-type current in KO/Lgi1, we recorded neurons in voltage-clamp to obtain D-type conductance. For the same voltage step, the outward DTx-k-sensitive current evoked was weak in KO/EGFP neurons but highly increased in KO/Lgi1 neurons to an extent that was similar to WT neurons (Fig. 4*A*). The D-type conductance was more than 2-fold in KO/Lgi1 neurons compared with the control (1.1 ± 0.4 nS, $n = 6$ in KO/EGFP neurons vs 2.8 ± 0.5 nS, $n = 8$ in KO/Lgi1 neurons, $p = 0.029$; Fig. 4*B*). The value of DTx-k-sensitive conductance reported in KO/lgi1 neurons was similar to that found in WT neurons (WT = 2.5 ± 0.2 nS, $n = 15$; Fig. 4*B*), indicating that Lgi1 rescue restored the D-type current.

In KO neurons, Kv1.1-containing channels were shown to be depleted mainly in the AIS (Seagar et al., 2017). We then evaluated Kv1.1-containing channel expression at the ankyrin G

(Ank G)-positive AIS of KO/EGFP neurons and KO/Lgi1 neurons (Fig. 4*C*,*D*). The Kv1.1 staining was colocalized with that of Ank G and was predominant at the AIS of WT and KO/Lgi1 neurons but not in KO/EGFP neurons (Fig. 4*C*). Overall, compared with KO/EGFP neurons, the normalized immunostaining of Kv1.1-containing channel at the AIS was significantly increased in KO/Lgi1 neurons (1.0 ± 0.1, $n = 17$ in KO/EGFP neurons vs 1.5 ± 0.1, $n = 19$ in KO/Lgi1 neurons, $p = 0.01$ and 1.8 ± 0.1, $n = 25$ in WT neurons; Fig. 4*D*), confirming that Lgi1 expression in CA3 neurons induced a D-type conductance recovery through a Kv1.1-containing channel rescue at the AIS.

Rescue of AIS length in KO/Lgi1 neurons

AIS length is subject to homeostatic regulation following activity deprivation or activity enhancement (Kuba et al., 2010; Jamann et al., 2021). AIS length measured by β4-spectrin immunostaining was found to be significantly shorter in KO-Lgi1 mice than in WT mice (22.6 ± 0.1 μm, $n = 98$ vs 35.2 ± 0.2 μm, $n = 72$; Mann–Whitney, $p < 0.0001$; Fig. 5*A*). This ~45% shortening of the AIS length suggests that the excitability increase observed in neurons lacking LGI1 (Seagar et al., 2017) is somehow compensated by an homeostatic process that makes the AIS shorter. We therefore checked whether restoring Lgi1 expression in neurons KO-Lgi1 neurons had an effect on AIS length. AIS length was found to be increased by ~27% in KO/Lgi1 neurons compared
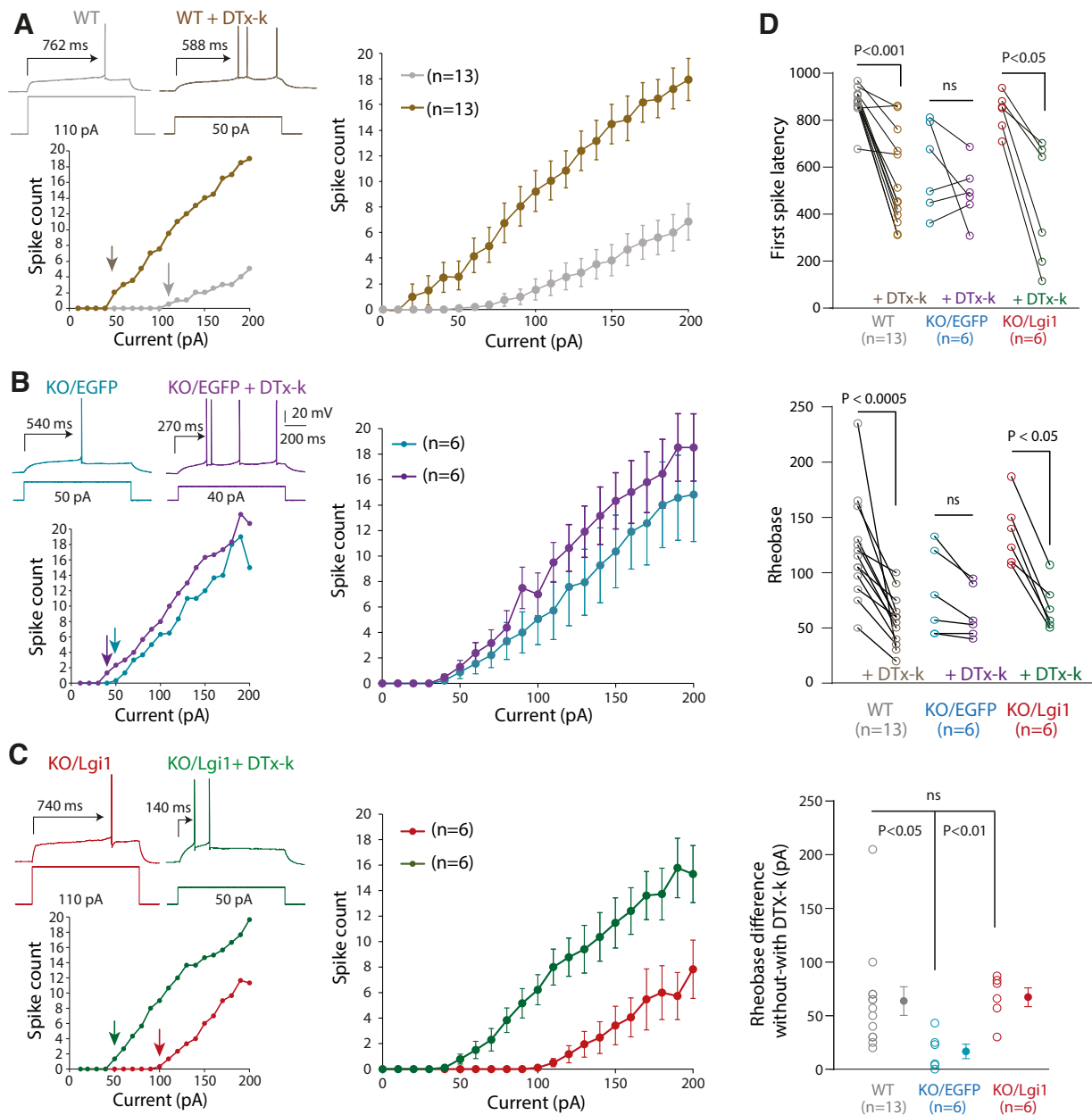
Figure 3. Rescued sensitivity to DTx-k in CA3 neurons electroporated with Lgi1 gene. *A*, Left, Input-output curves and corresponding traces of a WT (gray) representative neuron. DTx-k (100 nM) was bath-applied on WT neurons (brown-green). Rheobase is indicated on graph by arrows. Right, Averaged input-output curves. *B*, Left, Input-output curves and corresponding traces of a KO/EGFP representative neuron before (blue) and after (purple) bath application of DTx-k. Rheobase is indicated on graphs by arrows. Right, averaged input-output curves before and after bath application of DTx-k were obtained. *C*, Left, Input-output curves and corresponding traces of KO/Lgi1 representative neurons and right, averaged input-output curves before (red) and after (green) bath application of DTx-k. Right, Averaged input-output curves. *D*, Top, First spike latency obtained at rheobase current. Middle, Rheobase changes. Error bars represent SEM. Statistical analysis was performed using the Wilcoxon rank-signed test. Bottom, Effect of DTx-k on the rheobase. The DTx-k effect was obtained by subtraction of the rheobase after adding DTx-k to the rheobase before DTx-k and compared between KO/EGFP and KO/Lgi1. Error bars represent SEM. Statistical analysis was performed using the Mann–Whitney test and significance was obtained at $p < 0.05$. ns, not significant.

with KO/EGFP neurons ($28.3 \pm 1.9 \, \mu m$ vs $22.3 \pm 1.6 \, \mu m$, $n = 10$, Mann–Whitney test, $p = 0.03$; Fig. 5*B*). This result supports the view that Lgi1 rescue is sufficient to recover the length of the AIS in KO-Lgi1 mice (Fig. 5*C*).

Modulation of the excitability of adjacent neurons by LGI1 spillover

As LGI1 can be secreted by neurons (Senechal et al., 2005; Fukata et al., 2006; Lovero et al., 2015; Hivert et al., 2019), we checked the spatial extend of LGI1 rescue around an electroporated neuron. For this, CA3 neurons from KO-Lgi1 mice were

electroporated with a Dendra2-tagged LGI1 (D2-LGI1) encoding plasmid (Ramirez-Franco et al., 2022). To reliably evaluate the extracellular labeling of D2-LGI1 protein, antibodies against Dendra2 were applied on living organotypic cultures before fixation and permeabilization. In these conditions, the D2-LGI1 protein immunostaining was extracellular, confirming the ability of LGI1 to be secreted by CA3 neurons (Ramirez-Franco et al., 2022). D2-LGI1 was concentrated around the soma and mostly at the ankyrin G-positive AIS of the KO/D2-Lgi1 neuron. Moreover, we could follow the labeling of secreted D2-LGI1 protein all along the axon. The proximal basal and apical dendrites
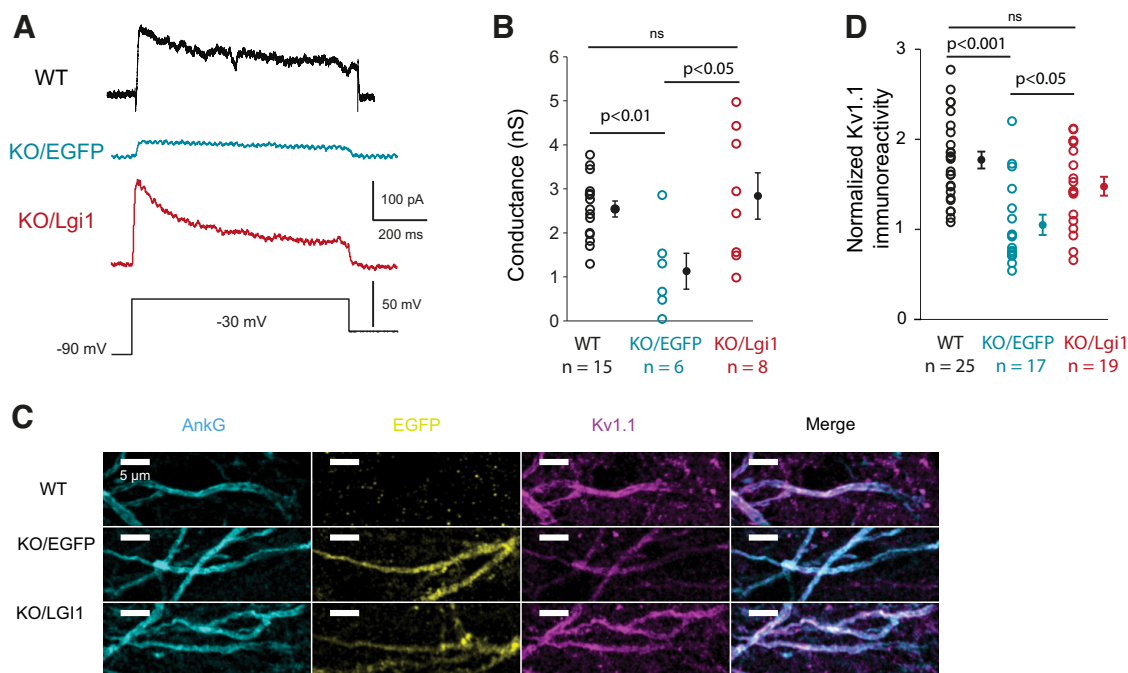
Figure 4. Rescue of the D-type current and Kv1.1 channels in CA3 neurons electroporated with Lgi1-expressing plasmid. ***A***, Representative traces of D-type current evoked by a voltage step from −90 to −30 mV in CA3 WT (top, black), KO/EGFP (blue), and KO/Lgi1 (bottom, red) neurons. ***B***, D-type conductance obtained in the three conditions. ***C***, Rescue of Kv1.1 channels at the AIS of CA3 neurons. Confocal images of immunostaining of Ank G (cyan), EGFP (yellow), and Kv1.1 (magenta) at the AIS of WT, KO/EGFP and KO/Lgi1 neurons. Overlapping of Ank G and Kv1.1 labeling appear in white on the merge images (last column). Arrows indicate starts and ends of the AIS. ***D***, Quantification of Kv1.1 immunoreactivity at the AIS of WT, KO/EGFP, and KO/Lgi1 neurons. Error bars represent SEM. ns, not significant.
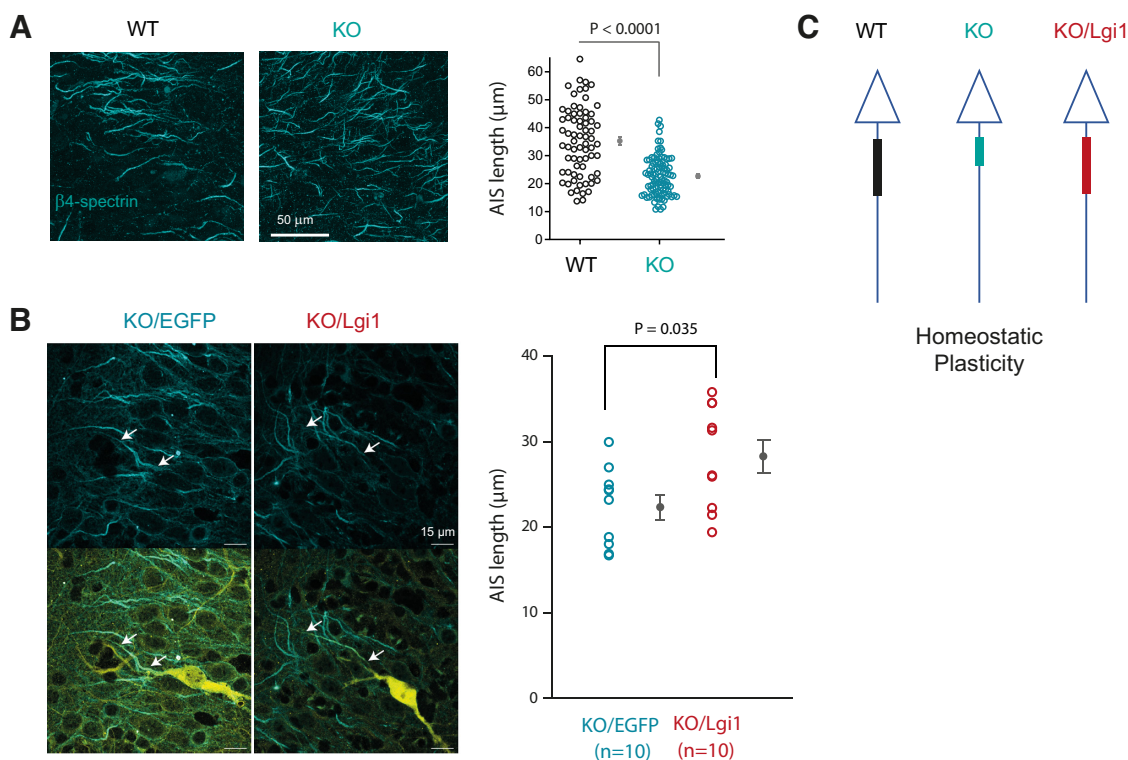

Figure 5. Rescue of AIS length in CA3 neurons electroporated with the Lgi1-expressing plasmid. ***A***, Reduction of the AIS length in neurons from Lgi1 KO mice compared with WT mice. β4-spectrin immunolabeling in WT (left image) and in Lgi1 KO mice (right image). Right panel, Group data (each dot represents one AIS). Statistical analysis was made using the Mann–Whitney test. ***B***, Comparison of AIS length in KO neurons electroporated with EGFP (left column) and with Lgi1 (right column). Note the elongation of the AIS in a KO neuron electroporated with Lgi1. Right panel, Group data. Statistical analysis was made using the Mann–Whitney test. ***C***, Summary scheme of the changes in AIS length as a function of Lgi1 expression.
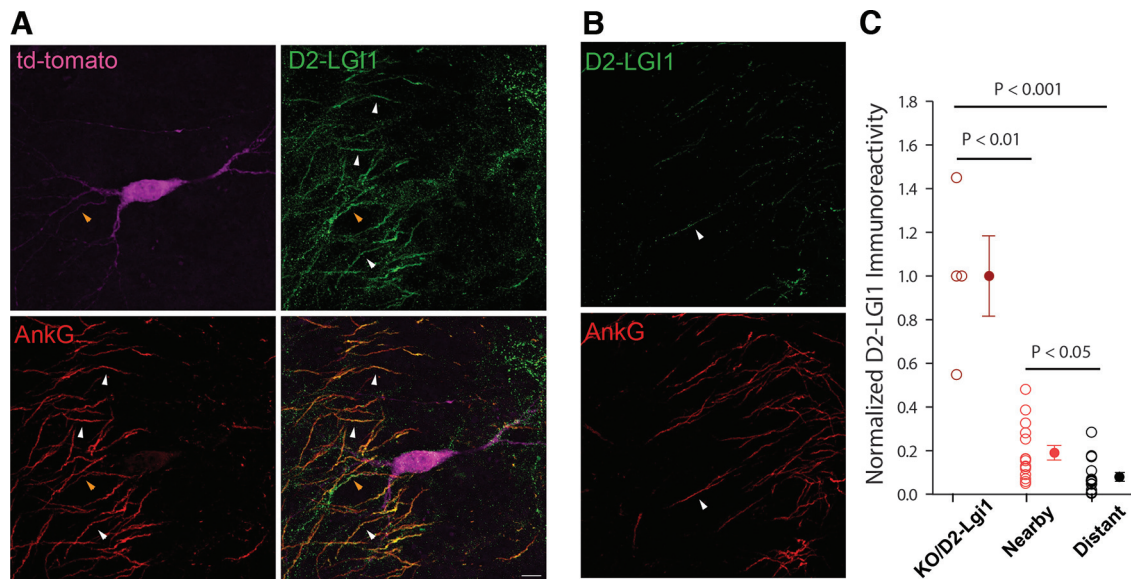
Figure 6. Spillover of LGI1 on adjacent neurons. *A*, tdTomato (magenta), Ank G (red), and D2-LGI1 (green) labeling are represented, with merge at the bottom corner for the field of view containing the KO/D2-Lgi1 neuron. Dotted frames indicate AIS chosen for the quantification. *B*, View at ~200 μm away from the KO/D2-Lgi1 neuron. *C*, Quantification of the D2-LGI1 immunoreactivity at the AIS of the KO/D2-Lgi1 neuron (dark red), nearby KO/D2-Lgi1 AIS (light red), and distant (black) neurons. Statistical analysis was made using the Mann–Whitney *U* test.

were also enriched in secreted D2-LGI1 so that dots of secreted D2-LGI1 form a cloud around the soma. No D2-LGI1 was detected around distant neurons >200 μm from the electroporated neuron. Remarkably, D2-LGI1 was also highly detected along the AIS of neurons adjacent to the AIS and basal dendrites of the KO/D2-Lgi1 neuron (Fig. 6A). To confirm that adjacent neurons to the electroporated neuron (i.e., nearby neurons) were targeted by the D2-LGI1, D2-LGI1 immunostaining was quantified at their AIS. D2-LGI1 immunostaining at the AIS of nearby neurons was ~20% that of KO/D2-Lgi1 neuron ($p < 0.01$; Fig. 6B,C) and a further reduction by half was observed for AIS located at >200 μm from the KO/D2-Lgi1 neuron ($p < 0.05$; Fig. 6B,C).

We then checked whether LGI1 extracellularly secreted by KO/Lgi1 neurons could affect the intrinsic excitability of nearby neurons (Fig. 7A). Randomly chosen KO neurons were recorded in current clamp within a 150 μm wide field around the KO/Lgi1 neurons. KO neurons recorded at a distance of >200 μm from the KO/Lgi1 neurons were chosen as a control. Intrinsic excitability of these distant KO neurons was similar to that of KO neurons recorded in nonelectroporated organotypic cultures (rheobase: 81 ± 9 pA, $n = 17$ vs 73 ± 3 pA, $n = 22$, $p = 0.5$; Figs. 2A, 7A). This confirms that neurons located far enough apart are not impacted by LGI1 secretion from the KO/Lgi1 neuron as suggested by the results of D2-LGI1 immunostaining. However, the input-output curve of nearby neurons presents a right shift that almost reach the curve of KO/Lgi1 neurons (Fig. 7A). Interestingly, rheobase of nearby neurons was significantly increased compared with the distant KO neurons (100 ± 7 pA $n = 25$ vs 73 ± 3 pA $n = 22$, $p = 0.003$; Fig. 7A) but also significantly decreased compared with KO/Lgi1 neurons (100 ± 7 pA $n = 25$ vs 129 ± 8 pA $n = 29$, $p = 0.01$; Fig. 7A). This result indicates that secreted LGI1 is able to modulate intrinsic excitability of nearby neurons.

As LGI1 protein rescued in KO/Lgi1 neurons allowed Kv1.1-containing channel recovery at the AIS, we measured Kv1.1 immunostaining at the AIS of nearby and distant neurons from KO/Lgi1 neurons (Fig. 7B). As expected, Kv1.1 immunostaining was significantly increased in KO/Lgi1 neuron compared with controls (1.48 ± 0.10 au $n = 19$ vs 0.99 ± 0.1 au; $n = 25$, $p = 0.002$; Fig.

7C). However, despite a trend in Kv1.1 immunostaining from distant to nearby to KO/Lgi1 neurons, no significant difference was measured between nearby and distant neurons (1.29 ± 0.15 au $n = 25$ vs 0.99 ± 0.10 au $n = 25$, $p = 0.14$; Fig. 7C). In addition, no significant difference in Kv1.1 immunostaining was observed between nearby and KO/Lgi1 neurons (1.29 ± 0.15 au $n = 25$ vs 1.48 ± 0.10 au $n = 19$, $p = 0.07$; Fig. 7C). Our results thus indicate that the partial rescue of the rheobase in nearby neurons could be because of an elevated level of Kv1.1 channels at the AIS by ~30%.

Discussion

We show here that rescuing Lgi1 expression in KO-Lgi1 CA3 pyramidal neurons reduces their intrinsic neuronal excitability and increases both the DTx-k-sensitive D-type current and the density of Kv1.1 channels at the AIS. KO/Lgi1 neurons displayed a higher voltage AP threshold and a higher rheobase that was similar to that found in WT neurons (Seagar et al., 2017). In addition, the sensitivity to DTx-k that is absent in KO/EGFP neurons was rescued in KO/Lgi1 neurons. Furthermore, the AIS length shortening observed in KO neurons is partially suppressed in KO/Lgi1 neurons. As LGI1 is a secreted protein, we also addressed here the spatial extent of the changes in excitability and Kv1 channel expression using the labeling of LGI1 with D2. We reveal a gradient of reduced excitability that is centered on the KO/Lgi1 neuron. Our results point to a major role of LGI1 in the control of Kv1.1 channels in the AIS of CA3 pyramidal neurons and thus open new strategies to treat epilepsies.

LGI1 determines intrinsic excitability through Kv1.1 channels

So far, the effects of Lgi1 deletion have been extensively explored on both cellular excitability and Kv1 channel expression. In fact, a reduction in both the D-type current and Kv1.1 channels at the AIS has been reported in KO CA3 pyramidal neurons (Seagar et al., 2017). In KO-Lgi1 pyramidal neurons of the cortex, cellular excitability is increased because of a reduction in the number of Kv1.2 (L. Zhou et al., 2018). Furthermore, the reduction in Lgi1 expression using RNA silencing methods has also revealed an
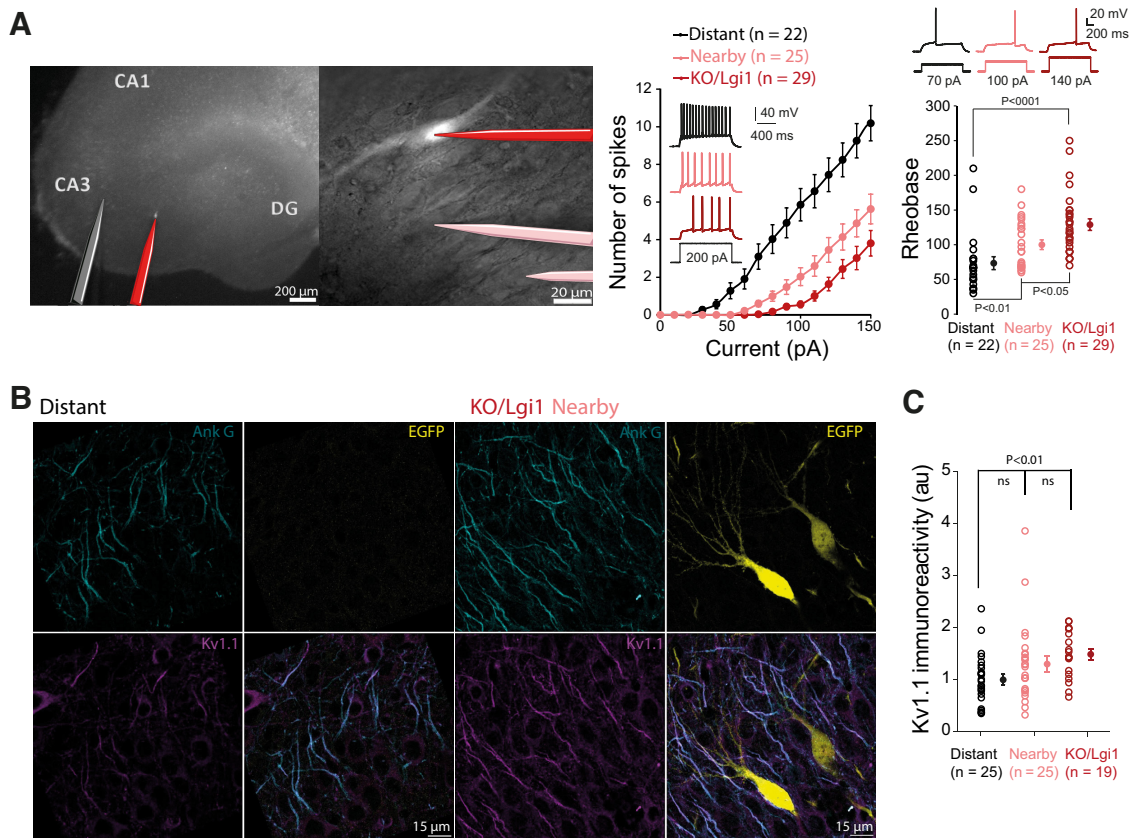
Figure 7. Paracrine reduction of intrinsic excitability induced by rescuing Lgi1 expression. ***A***, Hippocampal organotypic culture with a KO/Lgi1 neuron (left) and field of view of the KO/Lgi1 (right) with a scheme of the recording pipettes corresponding to distant (black), nearby (pink), and KO/Lgi1 (red) recorded neurons. Average input-output curves with corresponding traces and rheobase of the 3 conditions (bottom). ***B***, Immunostaining of AnkG (cyan), EGFP (yellow), and Kv1.1 (magenta) were represented in the field of view of distant and KO/Lgi1 neurons. ***C***, Quantification of Kv1.1 immunoreactivity at the AIS of distant, nearby and KO/Lgi1 neurons. Error bars represent SEM. Statistical analysis was performed using the Mann–Whitney U test. ns, not significant.

increase in neuronal excitability in dentate granule cells (Lugarà et al., 2020). We confirm here the link between LGI1 expression and Kv1 channel-dependent intrinsic excitability by showing that the rescue of Lgi1 expression reduces neuronal excitability through an elevation in the density of Kv1.1 channels and an enhancement of the DTx-k-sensitive D-type current.

Three lines of evidence support the fact that Kv1.1 channels are rescued in KO/Lgi1 neurons. First, the density of Kv1.1 channels was found to increase by 40% in KO/Lgi1 neurons. Second, the D-type current was increased by a factor 2 in KO/Lgi1. Third, the excitability was reduced (the spike threshold was elevated by ∼2 mV) and the sensitivity to DTx-k was restored. Taken together, our data demonstrate that LGI1 determines intrinsic excitability by controlling the expression of Kv1.1 channels at the AIS.

Kv1 channels are not only located at the AIS where they determine intrinsic excitability but they are also located at presynaptic terminals where they sharpen the spike and reduce transmitter release (Kole et al., 2007; Boudkkazi et al., 2011; Zbili et al., 2021). Interestingly, the upregulation of intrinsic neuronal activity in KO-Lgi1 CA3 pyramidal cells comes with a loss of Kv1 channel function at the presynaptic terminal (Seagar et al., 2017). The effect of LGI1 rescue on synaptic function has not been tested in the present study.

Rescue of AIS length
The AIS length was found to be reduced by ∼45% in KO mice compared with the WT. Such shortening in AIS length has been

already observed in status epilepticus induced with pilocarpine (Liu et al., 2017) and may therefore correspond to a homeostatic process (Turrigiano and Nelson, 2004; Grubb and Burrone, 2010; Kuba et al., 2010). Our study constitutes, however, the first report of an AIS shortening in a genetic model of temporal lobe epilepsy. We show that rescuing the Lgi1 expression in LGI1-deficient neurons was sufficient to partially suppress the AIS length shortening (the mean AIS length was 28 µm in KO/Lgi1 neurons vs 35 µm in wild-type neurons). Indeed, an increase by ∼27% was observed in electroporated neurons with the Lgi1-expressing plasmids. This partial rescue of the AIS length in KO/Lgi1 neurons could be attributable to a network effect. Indeed, the CA3 area is supposed to remain epileptic or at least hyperexcitable despite the restoration of LGI1 protein in single CA3 neurons. This result also suggests that homeostatic plasticity of the AIS length depends on both intrinsic and local circuit factors.

Spatial extent of paracrine release of LGI1
As LGI1 is a protein released by neurons, we used a D2-Lgi1 construct to show that LGI1 is mainly located at the AIS of the electroporated neuron and weakly present on the AIS of adjacent neurons. The excitability of neurons adjacent to the electroporated cell reveals a significant elevation of the rheobase in these neurons compared with that of more distant neurons. However, a nonsignificant increase in the Kv1.1 channel density (by ∼30%) was observed in KO neurons adjacent to KO/Lgi1 neurons, suggesting that electrophysiological analysis is more sensitive than immunostaining. Presynaptic and postsynaptic paracrine effects of LGI1 have been

reported on synaptic transmission (Lovero et al., 2015). AMPA/NMDA ratio recorded in KO-Lgi1 neurons neighbouring a neuron transfected with Lgi1 was similar to WT neurons. Furthermore, the AMPA/NMDA ratio recorded in KO-Lgi1 CA1 neurons that receive inputs from CA3 neurons that were previously transfected with Lgi1-expressing lentivirus, was identical to that of WT neurons (Lovero et al., 2015). However, in this study the spatial extent of the paracrine release of LGI1 was not tested. In conclusion, the rescue of intrinsic excitability in KO-Lgi1 pyramidal neurons is mediated by an upregulation of Kv1 channels in the AIS and is tightly controlled by Lgi1.

LGI1 is also expressed in astrocytes (Ramirez-Franco et al., 2022) and astrocytes are known to regulate extracellular levels of potassium ions that critically determine membrane potential and neuronal excitability. External potassium levels is controlled by Kir4.1 in astrocytes (Neusch et al., 2006). Downregulation of astrocytic Kir4.1 channels has been observed in a LGI1-deficient rat line that display audiogenic seizures (Kinboshi et al., 2019). Thus, a portion of the elevated excitability found in Lgi1−/− mice could be because of Kir4.1-deficiency in astrocytes.

Treatment of epilepsy

Hereditary epilepsy because of the lack of the LGI1 protein is rare but it has a high penetrance (Kalachikov et al., 2002). Genetic epilepsies are generally treated with anti-seizure medicine that pick out different targets. Our study opens new strategies to restore normal brain function in epileptic patients based on genetic tools. Treatment of inherited epilepsy has been made possible in mouse models of epilepsy using upregulation of Kv1.1-encoding gene with an *in vivo* CRISPRa strategy (Colasante et al., 2020). Our results strongly suggest that the restoration of normal neuronal excitability in epileptic patients, and therefore the cure of their epilepsy, is today conceivable through the re-expression of *lgi1* gene.

References

Boillot M, Lee C-Y, Allene C, Leguern E, Baulac S, Rouach N (2016) LGI1 acts presynaptically to regulate excitatory synaptic transmission during early postnatal development. Sci Rep 6:21769.

Bolte S, Cordelières FP (2006) A guided tour into subcellular colocalization analysis in light microscopy. J Microsc 224:213–232.

Boudkkazi S, Fronzaroli-Molinieres L, Debanne D (2011) Presynaptic action potential waveform determines cortical synaptic latency. J Physiol 589:1117–1131.

Chabrol E, Navarro V, Provenzano G, Cohen I, Dinocourt C, Rivaud-Péchoux S, Fricker D, Baulac M, Miles R, Leguern E, Baulac S (2010) Electroclinical characterization of epileptic seizures in leucine-rich, glioma-inactivated 1-deficient mice. Brain 133:2749–2762.

Colasante G, Qiu Y, Massimino L, Di Berardino C, Cornford JH, Snowball A, Weston M, Jones SP, Giannelli S, Lieb A, Schorge S, Kullmann DM, Broccoli V, Lignani G (2020) In vivo CRISPRa decreases seizures and rescues cognitive deficits in a rodent model of epilepsy. Brain 143:891–905.

Cudmore RH, Fronzaroli-Molinieres L, Giraud P, Debanne D (2010) Spike-time precision and network synchrony are controlled by the homeostatic regulation of the D-type potassium current. J Neurosci 30:12885–12895.

Debanne D, Boudkkazi S, Campanac E, Cudmore RH, Giraud P, Fronzaroli-Molinieres L, Carlier E, Caillard O (2008) Paired-recordings from synaptically coupled cortical and hippocampal neurons in acute and cultured brain slices. Nat Protoc 3:1559–1568.

Extrémet J, El Far O, Ankri N, Irani SR, Debanne D, Russier M (2022) An epitope-specific LGI1-autoantibody enhances neuronal excitability by modulating Kv1.1 channel. Cells 11:2713.

Fékété A, Ankri N, Brette R, Debanne D (2021) Neural excitability increases with axonal resistance between soma and axon initial segment. Proc Natl Acad Sci U S A 118:e2102217118.

Fukata Y, Adesnik H, Iwanaga T, Bredt DS, Nicoll RA, Fukata M (2006) Epilepsy-related ligand/receptor complex LGI1 and ADAM22 regulate synaptic transmission. Science 313:1792–1795.

Fukata Y, Lovero KL, Iwanaga T, Watanabe A, Yokoi N, Tabuchi K, Shigemoto R, Nicoll RA, Fukata M (2010) Disruption of LGI1-linked synaptic complex causes abnormal synaptic transmission and epilepsy. Proc Natl Acad Sci U S A 107:3799–3804.

Grubb MS, Burrone J (2010) Activity-dependent relocation of the axon initial segment fine-tunes neuronal excitability. Nature 465:1070–1074.

Hivert B, Marien L, Agbam KN, Faivre SC (2019) ADAM22 and ADAM23 modulate the targeting of the Kv1 channel-associated protein LGI1 to the axon initial segment. J Cell Sci 132:jcs219774.

Jamann N, Dannehl D, Lehmann N, Wagener R, Thielemann C, Schultz C, Staiger J, Kole MHP, Engelhardt M (2021) Sensory input drives rapid homeostatic scaling of the axon initial segment in mouse barrel cortex. Nat Commun 12:23.

Kalachikov S, Evgrafov O, Ross B, Winawer M, Barker-Cummings C, Martinelli Boneschi F, Choi C, Morozov P, Das K, Teplitskaya E, Yu A, Cayanis E, Penchaszadeh G, Kottmann AH, Pedley TA, Hauser WA, Ottman R, Gilliam TC (2002) Mutations in LGI1 cause autosomal-dominant partial epilepsy with auditory features. Nat Genet 30:335–341.

Kinboshi M, Shimizu S, Mashimo T, Serikawa T, Ito H, Ikeda A, Takahashi R, Ohno Y (2019) Down-regulation of astrocytic Kir4.1 channels during the audiogenic epileptogenesis in leucine-rich glioma-inactivated 1 (Lgi1) mutant rats. Int J Mol Sci 20:1013.

Kole MHP, Letzkus JJ, Stuart GJ (2007) Axon initial segment Kv1 channels control axonal action potential waveform and synaptic efficacy. Neuron 55:633–647.

Kuba H, Oichi Y, Ohmori H (2010) Presynaptic activity regulates Na(+) channel distribution at the axon initial segment. Nature 465:1075–1078.

Liu TT, Feng L, Liu HF, Shu Y, Xiao B (2017) Altered axon initial segment in hippocampal newborn neurons, associated with recurrence of temporal lobe epilepsy in rats. Mol Med Rep 16:3169–3178.

Lovero KL, Fukata Y, Granger AJ, Fukata M, Nicoll RA (2015) The LGI1-ADAM22 protein complex directs synapse maturation through regulation of PSD-95 function. Proc Natl Acad Sci U S A 112:E4129–E4137.

Lugarà E, Kaushik R, Leite M, Chabrol E, Dityatev A, Lignani G, Walker MC (2020) LGI1 downregulation increases neuronal circuit excitability. Epilepsia 61:2836–2846.

Neusch C, Papadopoulos N, Müller M, Maletzki I, Winter SM, Hirrlinger J, Handschuh M, Bähr M, Richter DW, Kirchhoff F, Hülsmann S (2006) Lack of the Kir4.1 channel subunit abolishes K+ buffering properties of astrocytes in the ventral respiratory group: impact on extracellular K+ regulation. J Neurophysiol 95:1843–1852.

Ollion J, Cochennec J, Loll F, Escudé C, Boudier T (2013) TANGO: a generic tool for high-throughput 3D image analysis for studying nuclear organization. Bioinformatics 29:1840–1841.

Rama S, Zbili M, Fékété A, Tapia M, Benitez MJ, Boumedine N, Garrido JJ, Debanne D (2017) The role of axonal Kv1 channels in CA3 pyramidal cell excitability. Sci Rep 7:315.

Ramirez-Franco J, Debreux K, Extremet J, Maulet Y, Belghazi M, Villard C, Sangiardi M, Youssouf F, El Far L, Lévêque C, Debarnot C, Marchot P, Paneva S, Debanne D, Russier M, Seagar M, Irani SR, El Far O (2022) Patient-derived antibodies reveal the subcellular distribution and heterogeneous interactome of LGI1. Brain 145:3843–3858.

Rathenberg J, Nevian T, Witzemann V (2003) High-efficiency transfection of individual neurons using modified electrophysiology techniques. J Neurosci Methods 126:91–98.

Schulte U, Thumfart J-O, Klöcker N, Sailer CA, Bildl W, Biniossek M, Dehn D, Deller T, Eble S, Abbass K, Wangler T, Knaus H-G, Fakler B (2006) The epilepsy-linked Lgi1 protein assembles into presynaptic Kv1 channels and inhibits inactivation by Kvbeta1. Neuron 49:697–706.

Seagar M, Russier M, Caillard O, Maulet Y, Fronzaroli-Molinieres L, De San Feliciano M, Boumedine-Guignon N, Rodriguez L, Zbili M, Usseglio F, Formisano-Tréziny C, Youssouf F, Sangiardi M, Boillot M, Baulac S, Benitez MJ, Garrido J-J, Debanne D, El Far O (2017) LGI1 tunes intrinsic excitability by regulating the density of axonal Kv1 channels. Proc Natl Acad Sci U S A 114:7719–7724.

Senechal KR, Thaller C, Noebels JL (2005) ADPEAF mutations reduce levels of secreted LGI1, a putative tumor suppressor protein linked to epilepsy. Hum Mol Genet 14:1613–1620.

Shaner NC, Campbell RE, Steinbach PA, Giepmans BNG, Palmer AE, Tsien RY (2004) Improved monomeric red, orange and yellow fluorescent proteins derived from Discosoma sp. red fluorescent protein. Nat Biotechnol 22:1567–1572.

Staub E, Pérez-Tur J, Siebert R, Nobile C, Moschonas NK, Deloukas P, Hinzmann B (2002) The novel EPTP repeat defines a superfamily of proteins implicated in epileptic disorders. Trends Biochem Sci 27:441–444.

Thomas RA, Gibon J, Chen CXQ, Chierzi S, Soubannier VG, Baulac S, Séguéla P, Murai K, Barker PA (2018) The nogo receptor ligand LGI1 regulates synapse number and synaptic activity in hippocampal and cortical neurons. eNeuro 5:ENEURO.0185-18.2018.

Turrigiano GG, Nelson SB (2004) Homeostatic plasticity in the developing nervous system. Nat Rev Neurosci 5:97–107.

Yamagata A, Miyazaki Y, Yokoi N, Shigematsu H, Sato Y, Goto-Ito S, Maeda A, Goto T, Sanbo M, Hirabayashi M, Shirouzu M, Fukata Y, Fukata M, Fukai S (2018) Structural basis of epilepsy-related ligand-receptor complex LGI1-ADAM22. Nat Commun 9:1546.

Yokoi N, Fukata Y, Kase D, Miyazaki T, Jaegle M, Ohkawa T, Takahashi N, Iwanari H, Mochizuki Y, Hamakubo T, Imoto K, Meijer D, Watanabe M, Fukata M (2015) Chemical corrector treatment ameliorates increased seizure susceptibility in a mouse model of familial epilepsy. Nat Med 21:19–26.

Zbili M, Rama S, Benitez M-J, Fronzaroli-Molinieres L, Bialowas A, Boumedine-Guignon N, Garrido JJ, Debanne D (2021) Homeostatic regulation of axonal Kv1.1 channels accounts for both synaptic and intrinsic modifications in the hippocampal CA3 circuit. Proc Natl Acad Sci U S A 118:e2110601118.

Zhou L, Zhou L, Su L, Cao SL, Xie YJ, Wang N, Shao CY, Wang YN, Zhou JH, Cowell JK, Shen Y (2018) Celecoxib ameliorates seizure susceptibility in autosomal dominant lateral temporal epilepsy. J Neurosci 38:3346–3357.

Zhou YD, Lee S, Jin Z, Wright M, Smith SEP, Anderson MP (2009) Arrested maturation of excitatory synapses in autosomal dominant lateral temporal lobe epilepsy. Nat Med 15:1208–1214.